Physica Medica 68 (2019) 124–131

Contents lists available at ScienceDirect

Physica Medica

journal homepage: www.elsevier.com/locate/ejmp

Original paper

Benchmarking a novel inorganic scintillation detector for applications in radiation therapy

Majed Alharbi[a,*], Michael Martyn[b], Sinead O'Keeffe[c], François Therriault-Proulx[d], Luc Beaulieu[d,e], Mark Foley[a,*]

[a] School of Physics, National University of Ireland Galway, Ireland
[b] Department of Medical Physics and Clinical Engineering, Galway University Hospitals, Galway, Ireland
[c] Optical Fibre Sensors Research Centre, University of Limerick, Ireland
[d] Departement de Radio-Oncologie and Centre de recherche du CHU de Quebec, CHU de Quebec, Quebec, QC G1R 3S1, Canada
[e] Departement de physique and Centre de recherche sur le Cancer, Universite Laval, Quebec, QC G1V 0A6, Canada

ARTICLE INFO

Keywords:
Inorganic scintillating detector
Hyperspectral technique
Cerenkov radiation
Band-pass filters
Monte Carlo simulations

ABSTRACT

Purpose: The aim of this study was to investigate the contribution of Cerenkov radiation to the overall signal measured with a novel inorganic scintillating detector (ISD).
Methods: An ISD based on terbium doped gadolinium oxysulphide (Gd_2O_2S:Tb) was used. A hyperspectral technique separated the Cerenkov signal from the radioluminescence (RL) signal of the ISD. The relative contribution of Cerenkov radiation was evaluated under different conditions. The efficiency of using simple spectral correction to reduce the Cerenkov contribution was quantified. Other experiments investigated were the dose-per-pulse dependence observed in our previous study and the absorbed-dose energy dependence when acquiring percentage depth dose curves using Monte Carlo (MC) simulations.
Results: The maximum relative contribution of Cerenkov radiation was 2.10% for a 10 × 10 cm^2 field at 10 cm depth. However, this percentage increased to 24% when the ISD was 7 cm out of field and exposed to a 10 × 10 cm^2 field. Using 15 nm and 5 nm band-pass filters reduced the Cerenkov contribution across all experimental conditions by a maximum of 75% and 82%, respectively. The MC simulation results show discrepancies between the measured and simulated PDD profiles using the Gd_2O_2S:Tb scintillator at depth.
Conclusion: This study showed that while Gd_2O_2S:Tb ISD provides high-signal intensity, the contribution of Cerenkov radiation under specific conditions can be significant. However, narrow band-pass filters can reduce the Cerenkov signal to a negligible level. The MC simulations suggest mechanisms other than the stem effect and the absorbed-dose energy dependence influence the response of the Gd_2O_2S:Tb scintillator measurements at depth.

1. Introduction

Detecting ionizing radiation using scintillation light is a long-established technique, and yet scintillator-based dosimetry in radiotherapy has not been commercially available until recently. Beddar et al. [1,2] conducted the first comprehensive study that used plastic scintillating fibres for dosimetry in radiotherapy, which is now viewed as the seminal work in this field [1,2]. Since that time, many research groups have focused on developing an optical fibre dosimetry system for external beam radiation therapy using both organic and inorganic scintillating materials [3–7]. One of the reasons for this focus is the introduction of new radiation therapy treatments techniques such as intensity modulated radiotherapy (IMRT) and volumetric modulated arc therapy (VMAT), which rely on small radiation field sizes and high dose gradients to deliver more conformal doses and tighter margins around tumours. These treatments techniques have caused well established dosimetry systems to be extended to their capability limits.

Moreover, international organizations, including the American Association of Physicists in Medicine (AAPM), recommend that in-vivo measurements be used to monitor radiotherapy treatments to determine any differences between the planned and delivered doses, which could be due to uncertainty encountered throughout the many steps of treatment planning and execution [8].

Optical fibre-based dosimetry provides several advantages compared to other systems that are currently in use for real-time in-vivo dosimetry including diodes, metal-oxide semiconductor field effect

* Corresponding authors.
E-mail addresses: m.alharbi2@nuigalway.ie (M. Alharbi), mark.foley@nuigalway.ie (M. Foley).

https://doi.org/10.1016/j.ejmp.2019.11.018
Received 1 July 2019; Received in revised form 29 October 2019; Accepted 18 November 2019
Available online 27 November 2019

transistors (MOSFETs) and electronic portal imaging devices (EPIDs). The advantages of optical fibre-based dosimetry include (i) real time radiation monitoring, (ii) small dimensions, (iii) immunity to electromagnetic fields and (v) linear response to doses and dose rate independency [9,10].

The Exradin W1 plastic scintillating detector (PSD) is the first commercial system based on scintillating optical fibres for dosimetry in radiotherapy [11], having been characterized for the first time by Beierholm et al. [4]. Due to their water equivalence, PSDs have been used for small field and in vivo dosimetry [12–16]. The reason why such a system was not used for dosimetry in external beam radiation therapy until recently was because of the light generated in the fibre optic cable when exposed to radiation, which is primarily attributed to Cerenkov radiation. Beddar et al. [1] introduced the term 'stem effect' to describe Cerenkov radiation and other light (fluorescence) that is produced in the fibre itself during irradiation [1].

Many techniques have been used in an attempt to reduce or eliminate the stem effect. Beddar et al. (1992) proposed using a background subtraction technique that employs two optical fibres placed parallel to each other; one with and one without scintillating materials [1]. By assuming that the fibre with no scintillating materials produces the same amount of Cerenkov radiation, the scintillation signal can be calculated by subtracting the two signals.

The temporal discrimination approach can be used for a slow scintillating material. In this case, measurements are taken after stem effect signal termination [17]. The most commonly used methods for determining Cerenkov radiation is the spectral discrimination technique. In this case, optical filters separate the green (in most cases) scintillation signal from the blue Cerenkov signal by taking advantage of the spectral differences between the two signals [5,6,18]. While the chromatic technique is efficient, it can only account for two component signals. Archambault et al. [19] generalized this technique to account for more than two light emitting sources [19]. Therriault-Proulx et al. [20] verified this using multi-point plastic scintillation detectors that use a single-fibre collection optical guide [20].

Recently, an inorganic scintillating detector (ISD) based on the inorganic scintillating material terbium doped gadolinium oxysulphide (Gd_2O_2S:Tb) was fabricated. This system has demonstrated promising characteristics when used in external beam radiation therapy settings [21]. However, the system overestimated the dose when measuring percentage depth dose (PDD) and lateral dose profiles; moreover, it showed dose per pulse dependence. With the possibility of accounting for the stem effect accurately, which has been proven to affect the accuracy of optical fibre-based dosimetry systems, it was the aim of this study to investigate the contribution of Cerenkov radiation to the observed over-response of the ISD system. The current study will contribute to the on-going research for new scintillators that can help optical fibre dosimetry systems to be routinely implemented for dosimetry in radiotherapy.

In this work, further results are reported on the characterisation of the ISD system introduced by Alharbi et al. [21]. We investigated the over-response of the ISD observed in our previous study by reporting the relative contribution of Cerenkov radiation to the overall signal of the ISD using the hyperspectral approach. The effect of use of high Z_{eff} material on the PDD measurements using Monte Carlo simulations was also investigated.

2. Methods and materials

2.1. Detector systems

The scintillating detectors used in this study were an ISD based on terbium doped gadolinium oxysulphide (Gd_2O_2S:Tb) supplied by Phosphor Technologies (UKL65/FR1) and a PSD (BCF-12) (Saint-Gobain Crystals, Hiram, OH, USA). The ISD was constructed using a polymethyl methacrylate (PMMA) plastic optical fibre. The core

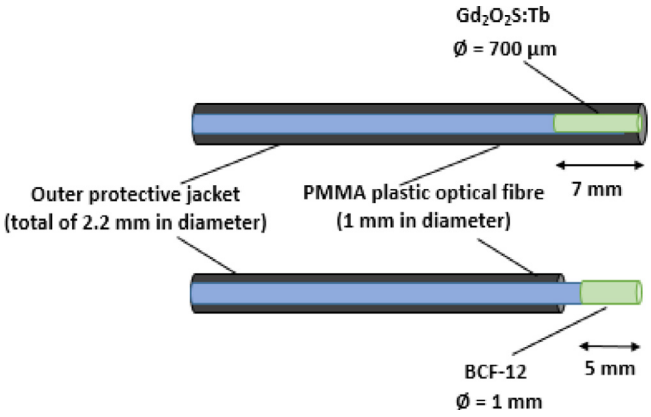

Fig. 1. Schematic of the two scintillating detectors used in this study, showing their composition and dimensions.

of the PMMA fiber was micro-machined to make a cavity with a 700 µm diameter and a 7 mm depth. The cavity was filled with the scintillating material and then sealed with an epoxy. The PSD was composed of a 5 mm long BCF-12 scintillating fibre coupled to a 15 m-long optical fibre (GH-4001, Mitsubishi, Tokyo, Japan), as shown in Fig. 1. The distal end of both detectors were attached with an SMA connector to QE65 Pro spectrometer (Ocean Optics, Dunedin, FL) cooled to −20C. The detector used in the spectrometer has a 1044 × 64 element CCD array from Hamamatsu and a wavelength acceptance range of 185–1100 nm. It was placed outside the treatment room to avoid interference from scattered radiation. The use of the spectrometer enabled us to access to the full spectrum of the incoming light and to use the hyperspectral approach for stem effect removal.

2.2. Hyperspectral filtration technique

The hyperspectral approach used in this study for stem-effect removal, follows the method previously described by Therriault-Proulx et al. [22]. As the hyperspectral technique uses spectral unmixing of the different light-emission sources (scintillator, stem-effect) instead of using the Cerenkov light ratio (CLR) approach, the irradiated fibre length does not need to be considered during the calibration procedure. When employing the hyperspectral approach, it is important to accurately determine the shape of the spectrum for each scintillators used in this study as well as the stem effect spectrum [19]. Therefore, at least five light spectra ranging from 324 to 1090 nm with a spectral resolution of 0.7 nm were obtained for the two scintillators and the bare fibre, as well as background spectra using the spectrometer. To remove unwanted noise in the spectra, median filtering was used for all measurements. The background spectra were subtracted from the scintillators signal spectrum for all measurements. Pure scintillating spectra were obtained by irradiating the two detectors with a 120 kVp x-ray beam, produced by a superficial therapy unit (Philips RT-250; Philips Corp., Eindhoven, Holland), in which production of Cerenkov light is impossible as the beam energy is below the Cerenkov production threshold of 178 keV in PMMA. The last step in the calibration process was to acquire the spectra of the stem effect using a 6 MV photon beam and 10x10 cm^2 field size. The bare fibre was positioned at D_{max} with 100 cm source to surface distance (SSD) and irradiated using 600 MU/min to deliver 50 MU for five measurements. All spectra were normalised to the area under the curve, as presented in Fig. 2.

3. Measurements

3.1. Spectral study

The contribution of the stem effect to the overall signal measured

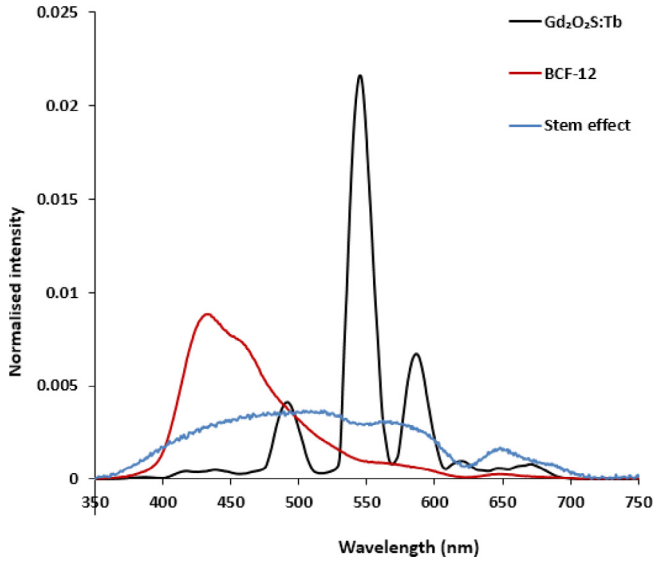

Fig. 2. The emission spectra (pure scintillating spectra) of the Gd_2O_2S:Tb, BCF-12 and the stem signal. Each spectra were acquired separately and normalized to the area under the curve.

with the ISD was investigated by evaluating the influence of the stem effect on the spectral shape of the radioluminescence (RL) spectrum of the Gd_2O_2S:Tb under different conditions. The measured 120 kVp x-ray spectrum (pure scintillating spectra) was used as a reference to detect any change in the spectral shape when using a 6 MV photon beam under different conditions including: different depths, different field sizes and out of field measurements. With no stem effect correction performed for these measurements, any change in the spectral shape of the RL spectrum with respect to the 120 kVp spectra can be attributed to the stem effect contribution. Two field sizes were used (2×2 cm^2 and 10×10 cm^2) and three different depths, 2 cm, 5 cm and 10 cm. The out of field measurements were performed using a 10×10 cm^2 field, with the ISD entering the field from one side (barely no optical fibre in the field) and leaving from the other end (optical fibre fully in the field), to represent worst case scenario where Cerenkov contribution at its highest value.

As the Gd_2O_2S:Tb scintillator has a narrow emission spectrum around 545 nm and produces higher signal intensities compared to organic scintillators, the feasibility of using simple spectral correction, where two narrow band-pass filters near the emission peak of the Gd_2O_2S:Tb signal to reduce the stem signal to negligible levels, was investigated. The two narrow band-pass filters: 15 nm (540–555 nm) and 5 nm (540–545 nm) were used and applied to all investigated conditions. Using such simple spectral correction for suppressing the stem signal could lead to more simplified detector systems for in vivo dosimetry in radiotherapy.

3.2. Dose per pulse dependence

To investigate the Dose per pulse (DPP) dependency of the ISD, the response of the ISD to different DPP values was measured using the spectrometer, and the results were then compared to the BCF-12 PSD detector. The different DPP values were obtained by using various SSD settings (75 cm–130 cm). For each measurement, 50 MU at 600 MU min^{-1} was delivered using a 6 MV photon beam, a 10×10 cm^2 radiation field size and the detectors were positioned in air at the beam isocentre. Measurements were repeated 5 times, and the results were normalized to that calculated at 100 cm SSD and compared to the BCF-12 results. The hyperspectral method was used to account for the stem effect.

4. Monte Carlo simulations

MC methods were employed to simulate the PDD dose profiles measured with the ISD in order to investigate the effect of using a high Z_{eff} scintillator on the energy dependence of the ISD in terms of absorbed-dose energy dependence.

4.1. Monte Carlo treatment head model tuning

The MC software packages BEAMnrc [23] and DOSXYZnrc [24] were used to develop a MC treatment head model of an Elekta Versa HD linear accelerator (linac). The BEAMnrc package was used to construct a virtual model of the 6 MV linear accelerator treatment head, while DOSXYZnrc was used for calculating dose distributions in a water phantom, with dimensions of $30 \times 30 \times 30$ cm^3; the phantom was positioned at an SSD of 90 cm. The treatment head model consisted of several components including: the x-ray target, primary collimator, flattening filter, tongue-and-groove multi-leaf collimator, and jaws. Linac treatment head specifications were provided by Elekta (under non-disclosure agreement with Elekta Oncology Systems, Crawley, UK). A 4-phase MC modelling process was used to achieve a reliable and accurate model across a large range of field sizes, in which the energy and the full width at half maximum (FWHM) of the incident electron beam were varied in steps of 0.1 MeV and 0.05 cm, respectively, in an iterative tuning process, [25–30]. The accuracy of the MC model was verified by comparing the simulated and measured commissioning lateral dose profiles and PDD curves, which were obtained using a PTW Semiflex 31,010 chamber and a PTW PinPoint 31,016 chamber across different radiation field sizes including 40×40 cm^2, 10×10 cm^2 and 2×2 cm^2. The electron and photon cut-off energies were set to 0.521 MeV and 0.010 MeV, respectively.

4.2. Monte Carlo simulation of the inorganic scintillating detector

PDD curves of the Gd_2O_2S:Tb scintillator were simulated using the MC user code DOSXYZnrc for two different field sizes: 10×10 cm^2 and 2×2 cm^2. The ISD was simulated with a $1 \times 7 \times 1$ mm^3 voxel of Gd_2O_2S:Tb with a density of 7.44 g cm^{-3}, which was positioned at a range of depths in a water phantom, to simulate the measurement conditions when acquiring the PDD curves. The results of the simulated profiles were then compared to physically measured PDD curves and those simulated in a homogeneous water phantom (i.e. without the ISD materials).

The EGSnrcMP code was used to generate the PEGS4 data for the Gd_2O_2S:Tb scintillator, using the parameters AP = 0.010 MeV, AE = 0.521 MeV in which AP and AE are the low-energy thresholds for the production of secondary bremsstrahlung photons and knock-on electrons, respectively.

5. Results and discussion

5.1. The stem effect on the ISD measurements

The impact of the stem effect on the spectral shape of the RL spectrum of the Gd_2O_2S:Tb under different conditions is presented in Fig. 3(A, B, C and D). The figure shows the pure RL spectra of the Gd_2O_2S:Tb obtained using a 120 kVp beam and the 6 MV spectra, where the stem effect would be present, plotted on the same axis after been normalised to the area under the curve for different conditions. As seen in the Figs (A and B), in standard conditions (i.e. in the centre of the field) there are no significant changes in the 6 MV RL spectral shape of the ISD due to the contribution of the stem effect. These results can be explained by the high scintillation yield of the Gd_2O_2S:Tb scintillator, which reduced the stem signal contribution to a maximum of 2.10% for 10x10 cm^2 field at a depth of 10 cm, as can be seen in Table 1. However, these changes in the RL spectra are evident when examining the

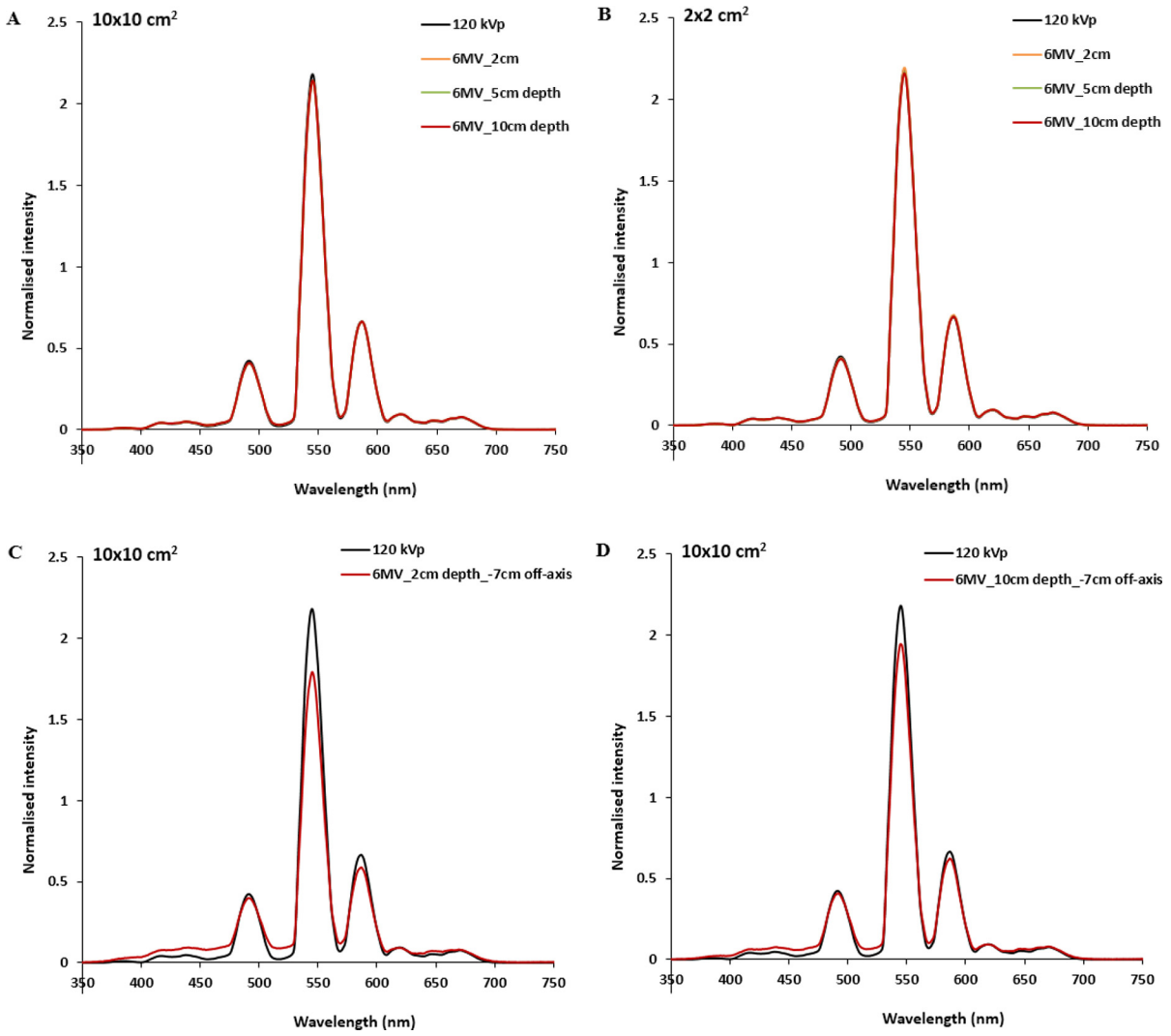

Fig. 3. The pure RL spectra of the Gd_2O_2S:Tb acquired using 120 kVp x-ray beam compared to spectra that is acquired using 6 MV beam under different experimental conditions: (A) 10 × 10 cm^2 field size at different depths; (B) 2 × 2 cm^2 field size at different depths; (C) out of field measurement (−7 cm) at 2 cm and (D) out of field measurement (−7 cm) at 10 cm depth.

Table 1
The relative percentage contribution of the stem effect to the overall signal measured with the ISD using two different field sizes at different depths.

Field size	Depth		
	2 cm	5 cm	10 cm
10 × 10 cm^2	0.06	0.27	2.10
2 × 2 cm^2	0.43	0.54	0.76

Table 2
The relative percentage contribution of the stem effect to the overall signal measured with the ISD using 10x10 cm^2 field sizes at different positions (infield and out of field).

Depth	ISD position			
	+7 cm	+3 cm	−3 cm	−7 cm
2 cm	0.98	2.22	3.33	24.00
5 cm	1.04	1.73	3.15	17.20
10 cm	1.24	1.39	3.34	13.53

spectra in the out of field measurements, presented in Fig. 3 (C and D). As would be expected, the influence of the stem effect on the spectral shape of the RL spectrum of the Gd_2O_2S:Tb increased with the increase in the amount of the optical fibre cable expose to the radiation field (i.e. for the −7 cm measurements, 10 cm of the optical fibre cable was exposed to the primary radiation beam).

A summary of the relative contribution of the stem effect signal to the ISD signal for 10x10 cm^2 and 2x2 cm^2 field at different depths and out of field measurements, is calculated using the hyperspectral method and presented in Tables 1 and 2. The maximum relative contribution of the stem effect to the ISD signal over all the investigated experimental conditions were 2.10%, 0.76%, 3.33% and 24.00% for 10x10 cm^2, 2x2 cm^2 at the centre of the field and 10 × 10 cm^2 at 3 cm and 7 cm away from the centre of the field, respectively. It is clear from the results that the contribution of the stem signal is minimal when measurements at the centre of the radiation field were considered due to the high light yield of the ISD [31,32]. It is also clear from Table 1 that the relative contribution of the stem effect increases as the field size and/or depth is increased. However, when the optical fibre cable was moved across the field a significant increase in the stem effect signal was measured. It should be noted that the later result represents a worst case scenario, where the scintillator is out of the radiation field with the optical fibre cable fully in the radiation field.

That being said, the use of a simple spectral correction for

Table 3
The relative percentage contribution of the stem effect to the overall signal measured with the ISD when using three different integrating methods for two field sizes at different depths.

Field size	Depth	Filtration method		
		Whole spectrum	15 nm filter	5 nm filter
10 × 10 cm^2	2 cm	0.06	0.02	0.01
	5 cm	0.27	0.07	0.05
	10 cm	2.10	0.54	0.36
2 × 2 cm^2	2 cm	0.42	0.11	0.07
	5 cm	0.54	0.14	0.09
	10 cm	0.76	0.19	0.13

Table 4
The relative percentage contribution of the stem effect to the overall signal measured with the ISD when using three different integrating methods for in-field and out of field measurements.

Depth	ISD position	Filtration method		
		Whole spectrum	15 nm filter	5 nm filter
2 cm	3 cm	0.97	0.25	0.17
	7 cm	2.17	0.57	0.38
	−3 cm	3.22	0.85	0.57
	−7 cm	19.35	5.80	3.98
5 cm	3 cm	1.03	0.27	0.18
	7 cm	1.70	0.44	0.30
	−3 cm	3.06	0.80	0.54
	−7 cm	14.67	4.23	2.89
10 cm	3 cm	1.22	0.32	0.21
	7 cm	1.38	0.36	0.24
	−3 cm	3.23	0.85	0.57
	−7 cm	11.92	3.35	2.29

suppressing the stem signal in all experimental condition was investigated and the results are shown in Tables 3 and 4. The results show the integration of the ISD signal over the acquired spectrum and comparing the result of using two different narrow band-pass filters, 15 nm (540–555 nm) and 5 nm (540–545 nm). It can be seen for the results that, using a 15 nm or 5 nm band-pass filter resulted in reducing the stem signal by a maximum of ~75% and 82% across all the investigated experimental conditions. This shows that using a combination of high RL scintillator and simple spectral correction could reduce the stem signal to negligible levels, which can lead to more simplified radiation detection systems in radiotherapy.

5.2. DPP dependence

The DPP values obtained with the ISD compared with those measured by the BCF-12 are shown in Fig. 4. Each DPP value was obtained at different SSD, normalized to the value calculated at 100 cm SSD and corrected for the stem effect using the hyperspectral technique. For all the DPP measurements, the ISD showed a minor DPP dependence with respect to the BCF-12 measurements with a maximum deviation of 1.2% at 80 cm SSD. This result conflicts with our previous study, in which we observed a high dependency of the ISD to high and low DPP values with a maximum deviation of 27 ± 0.68% at the highest dose value (SSD of 70 cm) and 7 ± 0.14% at low dose values (SSD of 130 cm) [21]. These results can be explained by the fact that we were using a Hamamatsu multi-pixel photon counter MPPC (C11208) in our previous study as a light detecting system, which can be a cheaper and easier to handle option for converting the optical signal from the detector to a processing unit. However, Chen et al. (2019) concluded that, while the MPPC (C11208) module is an excellent choice of photodetector due to its linearity, stability and high sensitivity, this module cannot be exposed to high intensity incident light levels (i.e. high radiation doses) as this can cause the system to be saturated [33]. They recommended monitoring the analogue output voltage during measurement after establishing the threshold voltage at which the MPPC was saturated. In contrast, the use of the spectrometer in this study gave the advantage of accessing the full light spectrum of the scintillators, where saturated wavelengths can easily identified and corrected for.

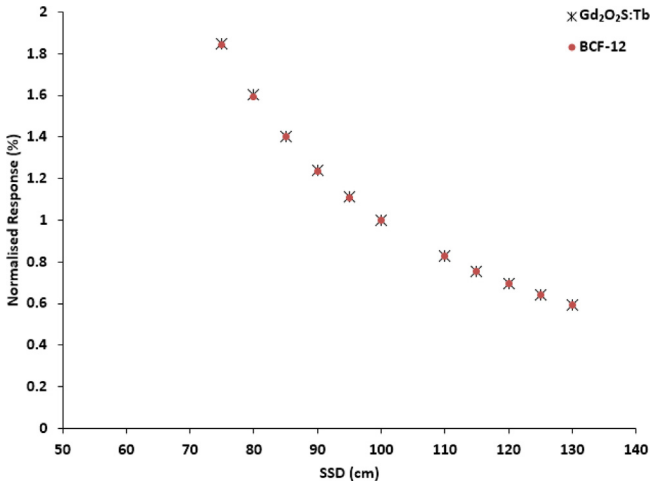

Fig. 4. Dose per pulse dependence for the ISD with respect to the BCF-12 PSD.

5.3. Monte Carlo model tuning

A MC treatment head model of the Elekta Versa HD linac was developed with incident electron beam peak energy of 6 MeV and FWHM of the beam radius of 0.30 cm along the x-axis and of 0.10 cm along the y-axis [25–30]. Fig. 5. shows normalized measured and MC calculated lateral dose profiles (x-axis) and PDD curves for field sizes of 40 × 40 cm^2, 10 × 10 cm^2 and 2 × 2 cm^2. For all lateral dose profiles and PDDs beyond D_{max}, measured and simulated values agree with < 2%, for all field sizes considered. The statistical uncertainty of all bins scoring more than 50% of the maximum absorbed dose was in all simulations < 1.0%. The tuned values of the primary electron beam were in good agreement with previously published studies. The model was used to simulate PDD dose profiles measured using the ISD.

5.4. Monte Carlo simulation of the inorganic scintillating detector

Fig. 6 shows the result of using the developed MC model to simulate the PDD profiles that were obtained using the ISD, using a 1x7x1 mm^3 voxel of Gd_2O_2S:Tb for two different field sizes, 10 × 10 cm^2 and 2x2 cm^2 and compared to the experimental data and MC simulation of a similar volume of water. The PDD profiles were simulated by calculating the absorbed dose in the scintillator voxel at different depths. A separate simulation was carried out for each depth. Each MC simulation was then normalized to the dose scored in the scintillator voxel from the simulation where it was positioned at D_{max}.

It is clear from the results that there are discrepancies between the measured PDD profiles and both MC simulated profiles, using a homogeneous water phantom and the Gd_2O_2S:Tb scintillator, in the build-up region for both field sizes used in this study. These differences can be explained by measurement uncertainties at a very high dose gradient region in addition to well documented and known limitations of using MC calculation in this region [34].

For the MC simulations in the homogeneous water phantom the percentage difference increases as a function of depth. However, the maximum percentage difference between the two profiles decreased with the decrease in field size from 16.8% and 6.6% for 10 × 10 cm^2 and 2 × 2 cm^2, respectively. This discrepancy can to some extent be attributed to the use of inorganic scintillating material (high Z_{eff}

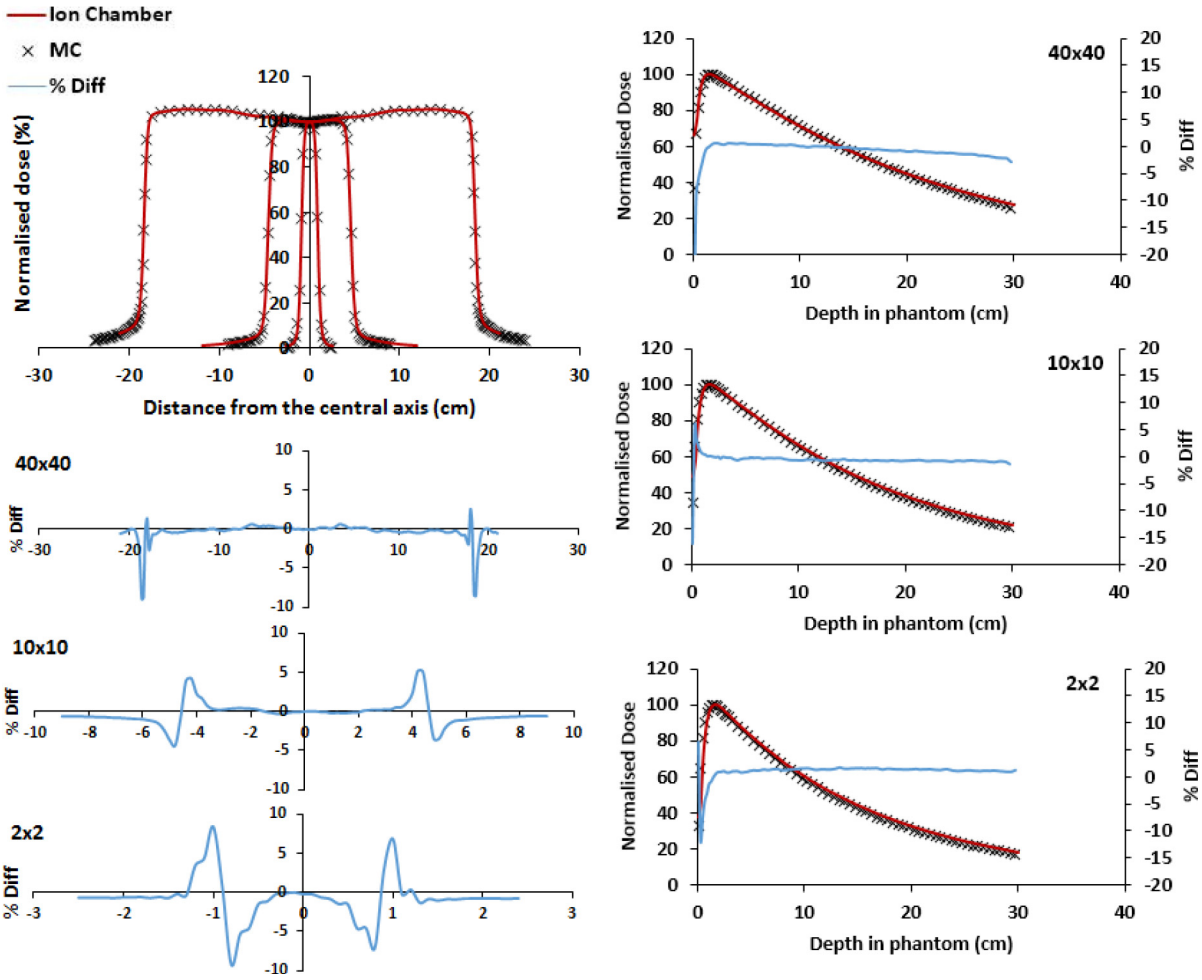

Fig. 5. Comparison of the MC simulated and ion chamber commissioning lateral dose profiles (left), with the percentage differences between measured and calculated dose values are shown at the bottom of the figures and PDD curves (right) for three different field sizes, (top) 40 × 40 cm^2, (middle)10 × 10 cm^2 and (bottom) 2 × 2 cm^2, normalized to D_{max}.

number) in the construction of the ISD. Studies by Molina et al. [36], Pittet et al. [35], Ramírez et al [37] and Martinez et al (2017) all show that ISDs overresponse with respect to ion chamber due to their sensitivity to low-energy radiation that is produced when the field sizes and/or the depth in phantom increases [7,35–37].

The MC simulated profile using the Gd_2O_2S:Tb scintillator differ from the MC simulated water profile for the 10x10 cm^2 field by a maximum of 5% at 10 cm depth, while, for the 2x2 cm^2 field the two profiles were in a very good agreement with a maximum of 0.5% difference at 10 cm depth. Again the differences observed in the 10x10 cm^2 can be explained by the sensitivity of the ISD to low energy radiation which becomes less important as the field size decreases. However, there are still significant differences between the measured and MC simulated profiles using the ISD for both field sizes investigated in this study. As the MC simulations only account for the absorbed-dose energy dependence (i.e. the high Z_{eff} number of the scintillating material), these differences suggest that there are other mechanisms (e.g. intrinsic energy dependence) that influence the response of the Gd_2O_2S:Tb scintillator when measurements at depth were considered other than the stem effect and the absorbed-dose energy dependence. Further investigations will be required to explore the cause of these discrepancies at depth.

6. Conclusion

In this study, the relative contribution of Cerenkov radiation to the observed over-response of the ISD system was investigated using the hyperspectral approach. We have demonstrated that the contamination of Cerenkov radiation cannot be negligible at all irradiation geometries in external beam radiation therapy. However, we showed that using 15 nm and 5 nm band-pass filters reduced the Cerenkov contribution across all experimental conditions by a maximum of 75% and 82%, respectively.

The DPP dependence results indicated that using the MPPC (C11208) as a light detecting system can affect the accuracy of the measurements when high radiation doses are used. The results of the MC simulations of the ISD showed that, using high Z_{eff} material caused the increase in the absorbed dose when field sizes and/or depths are increased. However, there is still a large discrepancy between the measured and simulated profiles using the Gd_2O_2S:Tb scintillator at depth. Further investigation is needed to study the scintillation mechanism that is responsible for the dose over-estimation of the ISD.

Acknowledgements

We would like to thank Elekta for providing us with the specifications required for modeling the linac treatment head. We wish to thank the Irish center for high end computing (ICHEC) for use of their supercomputer, which was an invaluable asset when running computationally intensive simulations. We would like to acknowledge the support of Peter Woulfe in the Galway Clinic. M. Alharbi. would like to acknowledge the Royal Embassy of Saudi Arabia for a Saudi Arabia

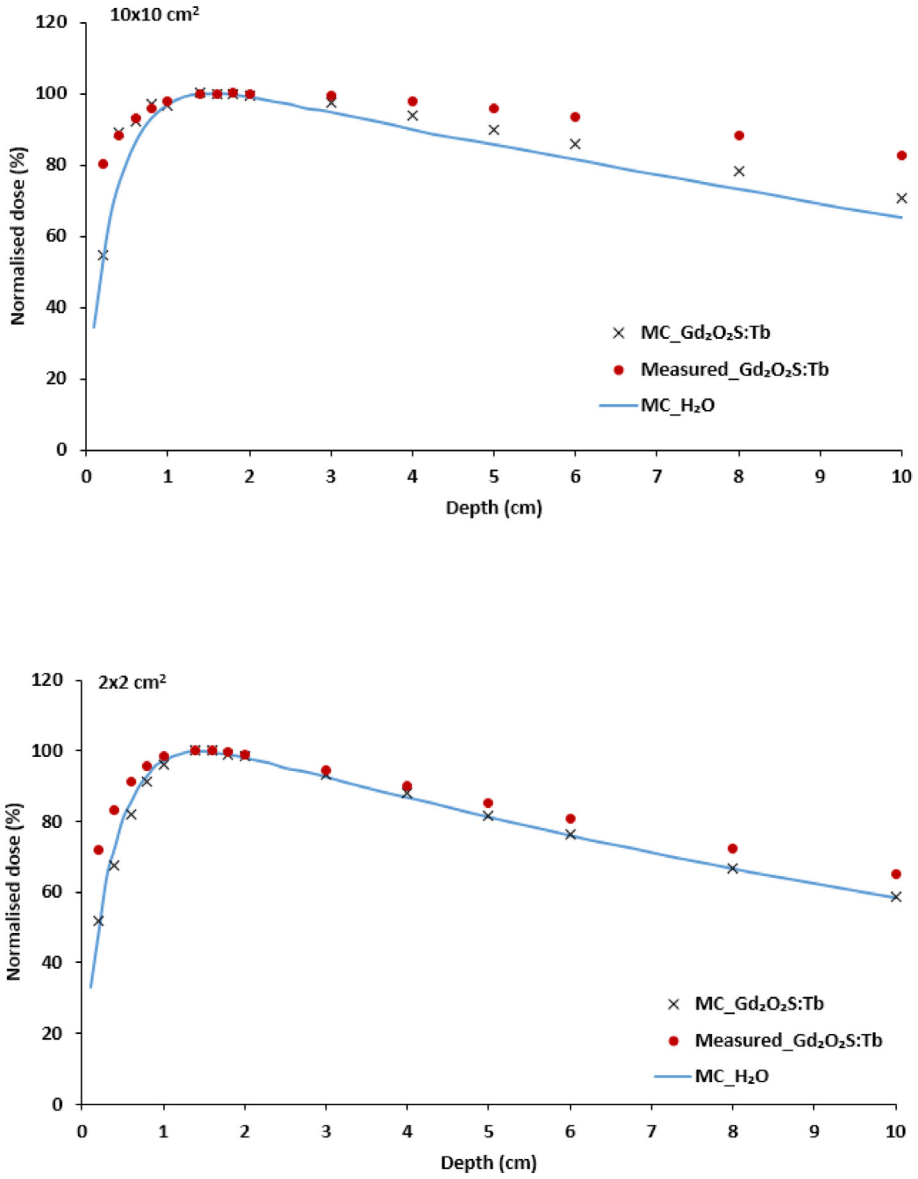

Fig. 6. Measured and simulated PDD profiles of the ISD. Simulated using 1x7x1 mm^3 Gd_2O_2S:Tb scintillating material (black crosses), measured using the ISD (red dots) and simulated using a similar volume of water (solid blue line) for two different field sizes, 10 × 10 cm^2 (top) and 2 × 2 cm^2 (bottom). (For interpretation of the references to colour in this figure legend, the reader is referred to the web version of this article.)

Government Scholarship.

References

[1] Beddar A, Mackie T, Attix F. Water-equivalent plastic scintillation detectors for high-energy beam dosimetry: I. Physical characteristics and theoretical considerations. Phys Med Biol 1992;37:1883.
[2] Beddar AS, Mackie T, Attix F. Water-equivalent plastic scintillation detectors for high-energy beam dosimetry: II. Properties and measurements. Phys Med Biol 1992;37:1901.
[3] O'Keeffe S, Grattan M, Hounsell A, McCarthy D, Woulfe P, Cronin J, et al. Radiotherapy dosimetry based on plastic optical fibre sensors. Fifth European Workshop on Optical Fibre Sensors: International Society for Optics and Photonics; 2013. p. 879418.
[4] Beierholm AR, Behrens CF, Andersen CE. Dosimetric characterization of the Exradin W1 plastic scintillator detector through comparison with an in-house developed scintillator system. Radiat Measur 2014;69:50–6.
[5] Fontbonne J, Iltis G, Ban G, Battala A, Vernhes J, Tillier J, et al. Scintillating fiber dosimeter for radiation therapy accelerator. Nuclear Science Symposium Conference Record, 2001 IEEE. IEEE 2001:1707–11.
[6] Guillot M, Gingras L, Archambault L, Beddar S, Beaulieu L. Spectral method for the correction of the Cerenkov light effect in plastic scintillation detectors: a comparison study of calibration procedures and validation in Cerenkov light-dominated situations. Med phys 2011;38:2140–50.
[7] Martínez N, Rucci A, Marcazzó J, Molina P, Santiago M, Cravero W. Characterization of YVO4: Eu3+ scintillator as detector for Fiber Optic Dosimetry. Radiat Measur 2017;106:650–6.
[8] Kutcher GJ, Coia L, Gillin M, Hanson WF, Leibel S, Morton RJ, et al. Comprehensive QA for radiation oncology: report of AAPM radiation therapy committee task group 40. Med phys 1994;21:581–618.
[9] Beaulieu L, Beddar S. Review of plastic and liquid scintillation dosimetry for photon, electron, and proton therapy. Phys Med Biol 2016;61:R305.
[10] O'Keeffe S, McCarthy D, Woulfe P, Grattan M, Hounsell A, Sporea D, et al. A review of recent advances in optical fibre sensors for in vivo dosimetry during radiotherapy. Br J Radiol 2015;88:20140702.
[11] Carrasco P, Jornet N, Jordi O, Lizondo M, Latorre-Musoll A, Eudaldo T, et al. Characterization of the Exradin W1 scintillator for use in radiotherapy. Med phys 2015;42:297–304.
[12] Mancosu P, Pasquino M, Reggiori G, Masi L, Russo S, Stasi M. Dosimetric characterization of small fields using a plastic scintillator detector: a large multicenter study. Phys Medica 2017;41:33–8.
[13] Therriault-Proulx F, Briere TM, Mourtada F, Aubin S, Beddar S, Beaulieu L. A phantom study of an in vivo dosimetry system using plastic scintillation detectors for real-time verification of 192Ir HDR brachytherapy. Med phys 2011;38:2542–51.
[14] Masi L, Russo S, Francescon P, Doro R, Frassanito MC, Fumagalli ML, et al. CyberKnife beam output factor measurements: a multi-site and multi-detector study. Phys Medica 2016;32:1637–43.
[15] Therriault-Proulx F, Beaulieu L, Beddar S. Validation of plastic scintillation detectors for applications in low-dose-rate brachytherapy. Brachytherapy

2017;16:903–9.
[16] Xue J, McKay JD, Grimm J, Cheng CW, Berg R, Grimm SYL, et al. Small field dose measurements using plastic scintillation detector in heterogeneous media. Med phys 2017;44:3815–20.
[17] Clift M, Johnston P, Webb D. A temporal method of avoiding the Cerenkov radiation generated in organic scintillator dosimeters by pulsed mega-voltage electron and photon beams. Phys Med Biol 2002;47:1421.
[18] Frelin AM, Fontbonne JM, Ban G, Colin J, Labalme M, Batalla A, et al. Spectral discrimination of Čerenkov radiation in scintillating dosimeters. Med Phys 2005;32:3000–6.
[19] Archambault L, Therriault-Proulx F, Beddar S, Beaulieu L. A mathematical formalism for hyperspectral, multipoint plastic scintillation detectors. Phys Med Biol 2012;57:7133.
[20] Therriault-Proulx F, Archambault L, Beaulieu L, Beddar S. Development of a novel multi-point plastic scintillation detector with a single optical transmission line for radiation dose measurement. Phys Med Biol 2012;57:7147.
[21] Alharbi M, Gillespie S, Woulfe P, Mccavana P, O'Keeffe S, Foley M. Dosimetric characterization of an inorganic optical fiber sensor for external beam radiation therapy. IEEE Sensors J 2019;19:2140–7.
[22] Therriault-Proulx F, Beaulieu L, Archambault L, Beddar S. On the nature of the light produced within PMMA optical light guides in scintillation fiber-optic dosimetry. Phys Med Biol 2013;58:2073.
[23] Rogers D, Walters B, Kawrakow I. BEAMnrc users manual. NRC Report PIRS. 2009; 509: 12.
[24] Walters B, Kawrakow I, Rogers D. DOSXYZnrc users manual. NRC Report PIRS. 2005; 794.
[25] Conneely E, Alexander A, Ruo R, Chung E, Seuntjens J, Foley MJ. Monte Carlo investigation of collapsed versus rotated IMRT plan verification. J Appl Clin Med Phys 2014;15:133–47.
[26] Conneely E, Alexander A, Stroian G, Seuntjens J, Foley MJ. An investigation into the use of MMCTP to tune accelerator source parameters and testing its clinical application. J Appl Clin Med Phys 2013;14:3–14.
[27] Martyn M, O'Shea T, Harris E, Bamber J, Gilroy S, Foley MJ. A Monte Carlo study of the effect of an ultrasound transducer on surface dose during intrafraction motion imaging for external beam radiation therapy. Med Phys 2017;44:5020–33.
[28] O'shea TP, Foley MJ, Faddegon BA. Accounting for the fringe magnetic field from the bending magnet in a Monte Carlo accelerator treatment head simulation. Med Phys 2011;38:3260–669.
[29] O'shea, TP, Foley MJ, Rajasekar D, Downes PA, Putten W, Moore M, et al. Electron beam therapy at extended source-to-surface distance: a Monte Carlo investigation. J Appl Clin Med Phys 2008;9:57–67.
[30] O'Shea TP, Ge Y, Foley MJ, Faddegon BA. Characterization of an extendable multi-leaf collimator for clinical electron beams. Phys Med Biol 2011;56:7621.
[31] Kertzscher G, Beddar S. Inorganic scintillation detectors based on Eu-activated phosphors for 192Ir brachytherapy. Phys Med Biol 2017;62:5046.
[32] Kertzscher G, Beddar S. Ruby-based inorganic scintillation detectors for 192Ir brachytherapy. Phys Med Biol 2016;61:7744.
[33] Chen LX, Ong YS, Chen SL, O'Keeffe S, Gillespie S, Woulfe P, et al. An LED PLD based controller for experimental characterization of an optical fibre sensor system for measurement of x-ray radiation in clinical linacs. Sensor Actuat a-Phys 2019;296:292–301.
[34] Chetty IJ, Curran B, Cygler JE, DeMarco JJ, Ezzell G, Faddegon BA, et al. Report of the AAPM Task Group No. 105: Issues associated with clinical implementation of Monte Carlo-based photon and electron external beam treatment planning. Med Phys 2007;34:4818–53.
[35] Pittet P, Ismail A, Ribouton J, Wang R, Galvan J-M, Chaikh A, et al. Fiber background rejection and crystal over-response compensation for GaN based in vivo dosimetry. Phys Med 2013;29:487–92.
[36] Molina P, Sommer M, Kattner F, Henniger J. Response characterization of an Y2O3: Eu-based radioluminescence probe under 60Co irradiation. Radiat Measur 2013;56:338–41.
[37] Ramírez M, Martínez N, Marcazzó J, Molina P, Feld D, Santiago M. Performance of ZnSe (Te) as fiberoptic dosimetry detector. Appl Radiat Isot 2016;116:1–7.